

## **Simulations of the Use of Cosmic-Rays to Image Nuclear Waste and Verify the Contents of Spent Fuel Containers - 11341**

**C. Jewett\*, V. N. P. Anghel\*, G. Jonkmans\*, M. Thompson\***

\*Atomic Energy of Canada Limited, Chalk River Laboratories, Chalk River, ON, Canada

### **ABSTRACT**

Researchers have used cosmic-ray muons to image the insides of large objects, such as Egyptian pyramids, since Luis Alvarez first used them to look for chambers within Chephren's pyramid in the late 1960s [1]. Muons are very much like electrons, except that they are about 200 times more massive. Cosmic-ray muons are some of the products of the interactions between primary cosmic-rays, such as protons, and the earth's upper atmosphere. Hence, they are a naturally occurring source of radiation. Due to their large mass and enormous momenta (3-4 GeV/c on average), they can penetrate several metres of rock before stopping. They also arrive at the surface of the earth at a rate of about 1 muon/min/cm<sup>2</sup>. In addition to these qualities, they also scatter more strongly in high-Z, high-density materials, such as uranium, than they do in low and mid-Z materials, like plastic and aluminum [2]. Thus, they make excellent probes of large structures.

More recently, a number of groups have extended the use of cosmic-ray muons to the imaging of cargo containers and nuclear waste containers [3][4][5][6][7]. This paper describes the results of Monte Carlo simulation studies of the multiple scattering and absorption of cosmic-ray muons traveling through a 55-gallon waste drum for nuclear material, and a Dry Storage Container (DSC) for spent CANDU<sup>1</sup> nuclear fuel. By using muon tomography and radiography techniques, images of the interiors of the drum and the DSC were generated. With these images, it was possible to identify the location of the uranium fuel pin in the 55-gallon drum. It was also possible to identify the locations of fuel bundles within the DSC, and also to see the absence of two columns of CANDU fuel bundles.

### **INTRODUCTION**

Cosmic-ray muons are a naturally occurring, abundant, and highly penetrating form of radiation. Various groups have exploited these properties in the application of cosmic-ray muon tomography and radiography to the imaging of the interiors of large structures. Luis Alvarez first pioneered the use of cosmic-ray muon radiography when he and his colleagues imaged the interior of Chephren's pyramid from 1967-1968 [1]. More recently, a number of groups have measured the trajectories of individual muons, in efforts to use muon tomography to detect smuggled Special Nuclear Materials (SNM) inside cargo containers, and to verify the contents of used-fuel containers for nuclear safeguards [3][4][5][6][7].

This paper describes simulation studies performed to determine the viability of the use of cosmic-ray muon radiography and tomography to verify the contents of used-fuel containers, and to characterise nuclear waste. These results will be applied to the use of cosmic-ray muon-based imaging as means to monitor nuclear fuel drums, to analyse the contents of radioactive waste containers, and to determine the integrity of fuel and container structures.

### **MUON TOMOGRAPHY**

Muon tomography entails the reconstruction of a three-dimensional image of the interior of an object, based on measurements of the initial and final trajectories of muons passing through it. Muon

---

<sup>1</sup> CANDU is a trademark of Atomic Energy of Canada Limited.

radiography, on the other hand, involves the creation of a two-dimensional image of the inside of an object, based on the measured, transmitted flux of muons traveling through it.

Muons, also a form of lepton, have the same properties as electrons, but are about 200 times more massive. Because of their large mass and large momenta (the average momentum is 3-4 GeV/c), when created in the upper atmosphere, they are capable of penetrating several metres of rock before stopping. When muons undergo multiple scattering in a lump of material, they emerge with an angular distribution that is approximately Gaussian, with a mean of zero, and a standard deviation given by Moliere's Equation:

$$\sigma_{\theta} = \frac{13.6MeV}{\beta cp} \sqrt{\frac{x}{X_0} \left[ 1 - 0.038 \ln \left( \frac{x}{X_0} \right) \right]} \quad (\text{Eq. 1})$$

where  $\beta cp$  is the speed $\times$ momentum of the muons, and  $x/X_0$  is the material thickness in units of its radiation length. The radiation length of a material decreases as its atomic number,  $Z$ , increases. Thus, one can use the measured RMS scattering angle of a collection of muons to determine whether they passed through a high-, mid- or a low- $Z$  material. For illustration, Table I provides the RMS scattering angles of 3 GeV muons, after traveling through 10 cm of some common materials [8].

Table I. The RMS scattering angles of 3 GeV muons, after traveling through 10 cm of some common materials. The RMS scattering angles were obtained with the Moliere Equation, and the radiation lengths and densities are from Ref [8].

Material	$X_0$ (g/cm <sup>2</sup> )	density (g/cm <sup>3</sup> )	$X_0$ (cm)	$\sigma_{\theta}$ (mrad)
<b>Water</b>	36.08	1.000	36.08	2.20
<b>Polypropylene</b>	44.77	0.900	49.7	1.85
<b>Concrete</b>	26.57	2.300	11.55	4.06
<b>Aluminum</b>	24.01	2.699	8.896	4.67
<b>Iron</b>	13.84	7.874	1.758	11.1
<b>Lead</b>	6.37	11.35	0.561	20.5
<b>Uranium</b>	6.00	18.95	0.317	27.9

A diagram of the basic muon tomography detector system, studied in this work, appears in Fig. 1. A basic muon tomography system consists of two tracker modules that sit above and below the object of interest. Each tracker module consists of two position-sensitive detectors, which measure two points on the muon's track. One uses the top two points, which the top module provides, to define the muon's initial trajectory, and the two bottom points to define the final trajectory. Given the initial and final trajectories, one can then calculate the muon's cumulative scattering angle. To determine the point at which the muon experienced the most scattering, one calculates the Points of Closest Approach (PoCAs) between the initial and final trajectory lines. The PoCAs are the points on each line that are closest to each other. Armed with the scattering angles and PoCAs of many muons that traveled through the object of interest, one can reconstruct a rough 2-dimensional image of its interior [9].

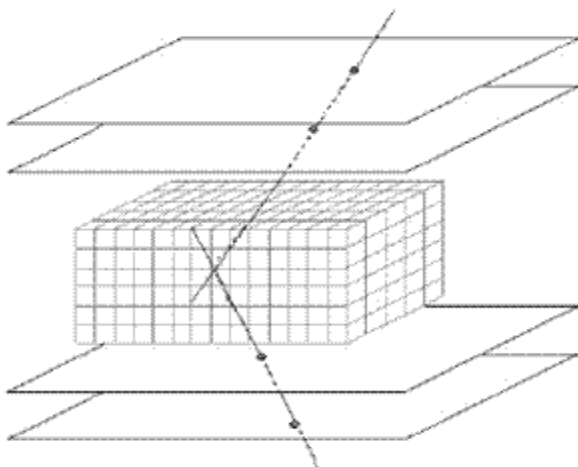


Fig. 1. A diagram of a muon tomography detector system and an object to be scanned by it [9].

## APPLICATIONS OF MUON TOMOGRAPHY

### Radioactive Waste Management and Nuclear Waste Characterisation

Improper handling and disposal of radioactive waste threatens public health, the environment, and the safety of workers. Hence, it is important to have effective radioactive waste management programs. Many radioactive waste programs segregate and characterise radioactive waste. Atomic Energy of Canada Limited (AECL) has had a nuclear waste management program since its laboratories began operation in 1945.

AECL's waste management program engages in the following activities: 1) research and development (R&D) to determine the best geological locations and methods for disposal of Canada's nuclear used-fuel waste, 2) interim period dry storage of nuclear waste, 3) the transportation and storage of liquid waste, 4) fuel packaging and storage, and 4) decommissioning activities at Chalk River Laboratories and Whiteshell Laboratories. AECL's nuclear waste is a product of its nuclear R&D activities and medical isotope production [10][11].

Radioactive waste possesses a plethora of physical, chemical and radiological properties. Multiple approaches must be adopted to deal with the multitudes of nuclear waste types. As Reference [12], along with the other references it cites, state, emerging methods of waste characterisation are assisting in the proper long-term disposal or storage of nuclear waste. Nuclear waste appears in two categories, based upon its characterisation history. *New waste* is nuclear waste that has been, and will be characterised by a characterisation program throughout its lifecycle. *Historical waste*, according to IAEA standards [12], is waste that lacks a comprehensive, traceable waste characterisation program. Historical waste is not necessarily older than new waste; it merely lacks the characterisation record that new waste possesses. Because of the lack of characterisation history of historical waste, it is much more difficult to store or dispose of it properly. Table II, taken from Reference [12], lists a variety of waste types, their levels of complexity, and whether or not they are stable. Two waste features that determine how an effective waste characterisation program must operate are 1) the complexity of the waste and 2) the stability of the waste. The waste's complexity is the number of properties that define its fingerprint. The stability of the waste is determined by the extent to which its properties evolve with time. The complexity and stability of the container holding the waste are also important elements which an effective waste management program must address. In the end, the fingerprint of nuclear waste and its container consists of their radioactivity, chemical, physical, mechanical, thermal and biological properties, and how they change with time.

Table II. Classification of waste streams by ease of measurement and sampling ability.

Traceable Waste Stream:	Simple & Stable	Complex & Stable	Simple & Variable	Complex & Variable
Nuclear Power Plant	x	x		
Institutional	x			
Nuclear Research Laboratory			x	
Reprocessing		x		
Enrichment, Conversion, Fuel Fabrication	x			
Decommissioning	*	*	*	*
Spent Sealed Source	x			
Spent Fuel	x			
Final Waste Form		x		
Non-Traceable Waste Stream:				
Historical	**	**	**	**

\* Facility dependent

\*\* may or may not include this subtype

The following list is an important subset of the nuclear waste characterisation challenges and issues that Reference [12] describes:

- Historical waste. Characterising waste from a non-traceable waste stream is more difficult. One can distinguish amongst different types of waste. Examples of these waste types include liquid-filled tanks, waste/work areas that must be decontaminated before decommissioning, and interim waste storage sites.
- Some forms of waste are difficult or even impossible to measure and characterise with existing technology. Examples include encapsulated alpha/beta emitters and heavily shielded waste.
- Some waste can only be measured with Non-Destructive Assay (NDA) techniques. Unfortunately, NDA techniques often do not provide conclusive information.
- It is often necessary to determine the level of homogeneity of waste, and also to determine its composition. For example, sludge in tanks and in-homogeneities in cemented waste need to be characterised.
- Assessment of the condition of the waste and its container is also crucial. Examples of problems with the condition of waste and its container include breach of containment, corrosion, and voids [12].

This work investigated the use of muon tomography and muon radiography to help characterise nuclear waste.

## SIMULATIONS

The GEANT4 simulation package was used to simulate the passage of muons through both a 55-gallon drum, filled with polyethylene (PE), and containing one CANDU™ fuel pin, and a Dry Storage Container (DSC). GEANT4 is a Monte Carlo simulation package that models a wide variety of particle processes, and the interactions of particles with matter. One of GEANT4's assets is the fact that it gives the user control over the main aspects of the simulation. These aspects are the simulation geometry, particles, run action, events, detector responses, physical processes, and transparent access to cross-sections. One can find more information about GEANT4 in Reference [13].

## Simulation Geometries

The simulation detectors consisted of a top and a bottom plane, each of which was 1 cm thick, and was made of argon gas at standard temperature and pressure (STP). These detectors were “perfect” detectors, since they provided perfect position and momentum vector information for each muon, when it crossed the argon planes. These detectors also only registered the presence of muons, despite the fact that, in reality, the passage of a muon through a container creates showers of other particles.

For the 55-gallon drum simulations, the drum was centred between the top and bottom argon planes, which were 2 m long by 2 m wide. The walls of the drum were 1.7 mm thick, and were made of GEANT4’s NIST Manager iron. The drum was 83.82 cm high, and it had a radius of 57.15 cm. The PE, which was GEANT4’s NIST compound, G4\_PARAFFIN, had a density of 0.93 g/cm<sup>3</sup>. The fuel pin, which was composed of 10 g/cm<sup>3</sup> UO<sub>2</sub>, had a radius of 0.5 cm and a length of 10 cm. The fuel pin sat off-centre within the PE, and was aligned with the central axis of the drum. To simulate a breach of containment, a 5 cm radius void was also added to the PE.

A diagram of the DSC model that was used in the GEANT4 simulations appears in Fig. 2. In the image on the left all 384 of the UO<sub>2</sub> fuel bundles, which appear in cyan, are present. Each fuel bundle 49.53 cm long and had a radius of 5.1 cm. The top and bottom detector planes appear in translucent yellow, and the 2.12 m × 2.15 m × 3.55 m DSC structure, with 1.3 cm thick iron walls, and 52 cm thick concrete (2.3 g/cm<sup>3</sup>) shielding, appears as a white wireframe. In the righthand image, two columns of fuel bundles are missing.

## Simulations of the Muons’ Tracks

Cosmic-ray muons arrive at the surface of the earth, at sea level, at a rate of about 1 muon/min/cm<sup>2</sup> [2]. The incident polar angles of these muons follow a  $\cos^2\theta$  distribution [14], which was included in the particle generator code of the simulations. In 1995, a group of researchers used the Balloon-borne Experiment with a Superconducting Spectrometer (BESS) to measure the energy spectrum of cosmic-ray muons at Tsukuba, Japan. The measured BESS spectrum ranged from 0.576 GeV/c to 20.552 GeV/c. The GEANT4 simulations that this paper describes used the Tsukuba 1995 BESS spectrum for  $\mu^+$  to generate the muons’ energies [15]. While the significant particle types, such as gammas, leptons, neutrons, protons and low mass mesons, were declared, only the most prominent processes were registered to the particles. For muons, the simulation registered only the multiple scattering, ionisation, bremsstrahlung and pair production processes.

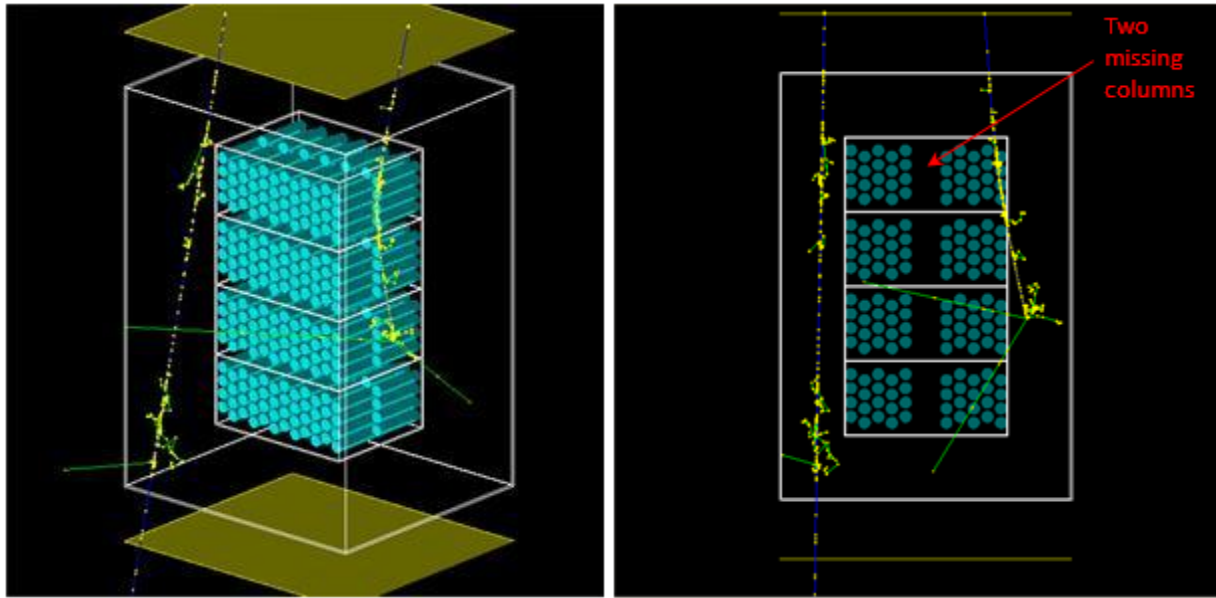


Fig. 2 The image to the left is a rendering of the DSC model used in GEANT4. The tracks of two muons appear in blue, along with the secondary gamma-rays produced by them, which appear in green. The image to the right is a wireframe view of the DSC model, with missing two columns of fuel bundles.

## CALCULATIONS AND ANALYSIS

### Muon Tomography

For the muon tomography analyses, the cumulative scattering angle and PoCAs of each muon track that passed through the object of interest were calculated from the top and bottom hit positions and momentum vectors that the argon tracker planes provided. The scattering angle was calculated simply by using the following formula:

$$\theta = \cos^{-1} \left( \frac{\mathbf{p}_i \cdot \mathbf{p}_f}{\sqrt{p_i^2 p_f^2}} \right) \quad (\text{Eq. 2})$$

where  $\mathbf{p}_i$  and  $\mathbf{p}_f$  are the muon's initial and final momentum vectors.

The calculations of the PoCAs were a bit more involved, and were based upon the fact that the shortest line connecting two trajectory lines is perpendicular to both of them. First, one begins by expressing the initial and final trajectory lines as

$$\mathbf{L}_i(s) = \mathbf{r}_i + s\mathbf{u}_i \quad (\text{Eq. 3})$$

$$\mathbf{L}_f(t) = \mathbf{r}_f + t\mathbf{u}_f \quad (\text{Eq. 4})$$

$\mathbf{L}$  is the trajectory line vector,  $\mathbf{r}$  is the first point on the line,  $\mathbf{u}$  is the unit direction vector of the line, and  $s$  and  $t$  are the displacements along the lines. A line connecting  $\mathbf{L}_i$  to  $\mathbf{L}_f$  is  $\mathbf{w} = \mathbf{L}_i - \mathbf{L}_f$ . Exploiting the fact that the shortest  $\mathbf{w}$  is perpendicular to both  $\mathbf{L}_i$  and  $\mathbf{L}_f$ , one can take the cross products of  $\mathbf{w}$  with  $\mathbf{L}_i$  and  $\mathbf{w}$  with  $\mathbf{L}_f$  to obtain two equations in two unknowns, where the unknowns are  $s_{\text{PoCA}}$  and  $t_{\text{PoCA}}$ .

$$\mathbf{w} \times \mathbf{L}_i = \mathbf{w} \times \mathbf{r}_i + \mathbf{w} \times s_{PoCA} \mathbf{u}_i = 0 \quad (\text{Eq. 5})$$

$$\mathbf{w} \times \mathbf{L}_f = \mathbf{w} \times \mathbf{r}_f + \mathbf{w} \times t_{PoCA} \mathbf{u}_f = 0 \quad (\text{Eq. 6})$$

After solving for  $s_{PoCA}$  and  $t_{PoCA}$ , one can then insert them into the equations for  $\mathbf{L}_i$  and  $\mathbf{L}_f$  to obtain the two PoCAs on the lines. To create an image of the interior of the object of interest from the PoCAs and scattering angles of the muon tracks, one needs only to plot the scattering angle as a function of the two PoCA positions.

## Muon Radiography

A muon radiography analysis was only performed for the simulations of the DSC. Muon radiography involves measuring the transmitted flux of a parallel beam of muons. It is possible to achieve the parallel beam effect by measuring the hit positions of muons in the top and bottom detectors, and only including muons that had hit positions in the same horizontal cells in the top and bottom detectors. In essence, a muon event was only included if its hit position in the bottom detector was in a 5 cm  $\times$  5 cm cell directly below the cell it hit in the top detector.

## RESULTS

### Muon Tomography

A reconstructed image of the interior of the simulated 55-gallon drum appears in Fig. 3. 400,000 cosmic-ray muons, the equivalent of a day's worth of muons, were thrown at the top detector. Only the muons that passed through two detectors and the drum, and that had scattering angles greater than 1.7 mrad, entered into the generation of this image. A cluster of white points clearly demarks the location of the fuel pin within the drum. As one can see from the figure, muon tomography utilizing only the cumulative scattering angle and the two PoCA points of each muon that traversed the object of interest works very well for cases in which only a small amount of high-Z material is present in a container, filled with low-Z material. However, as was found in the case of the DSC simulations, this approach does not produce clear images of the insides of containers possessing large amounts of high-Z material.

The large stopping powers and short radiation lengths of high-Z materials are the causes of the poor image quality that simple PoCA-based muon tomography yields for objects containing large quantities of high-Z, high density materials. The short radiation length (less than 1 cm) of a high-Z material, results in a tendency for the muons to undergo continuous, large angle scattering as they transit it. If the bulk of the high-Z material is great enough, the continuous, large angle scattering of the muons will tend to smear their PoCAs all over the regions containing the high-Z substance. The large stopping power of large amounts of high-Z, high density material also significantly reduces the number of muons that survive passage to the bottom detector. The large stopping power thus creates a large decrease in the number of measured PoCAs associated with high-Z bodies. The decrease in the relative number of measured PoCAs, associated with high-Z objects, along with the smearing of the PoCAs, damages the quality of images of the object's interior, and results in an inability to pinpoint the presence or absence of individual high-Z objects, such as fuel pins.

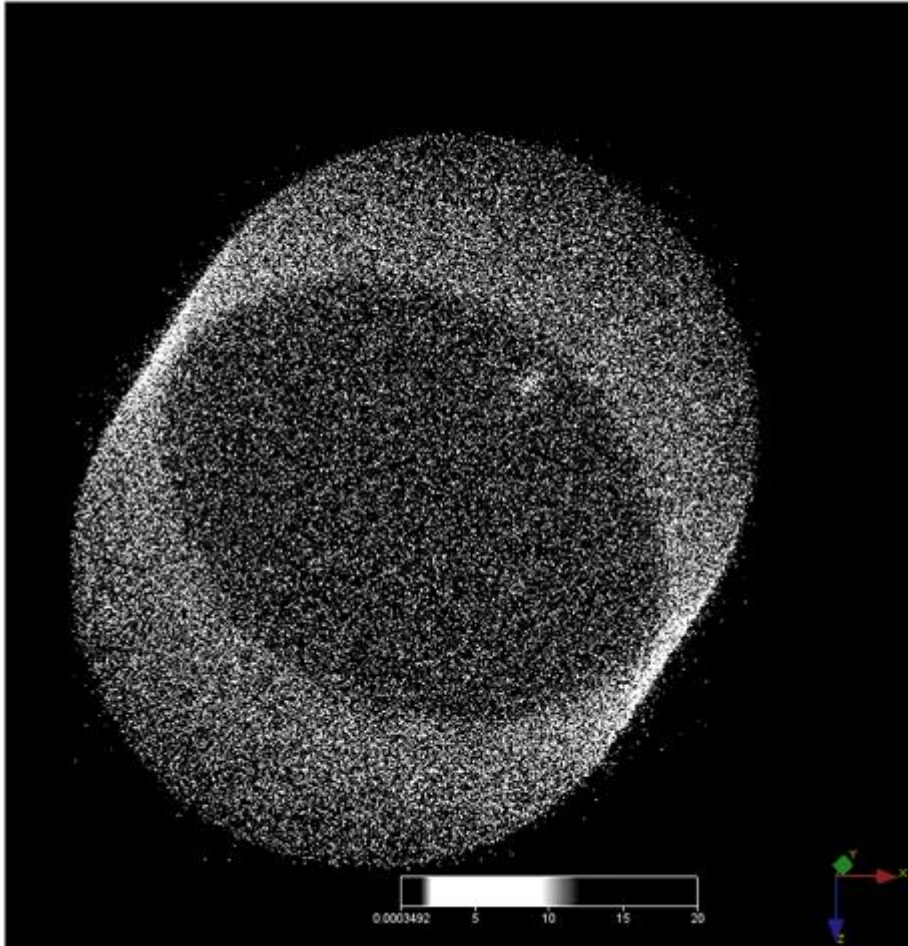


Fig. 3. Reconstructed image of a 55-gallon drum with a UO<sub>2</sub> fuel pin in paraffin.

### **Muon Radiography**

While the tendency for large amounts of high-Z materials to cause large angle scattering of muons is a liability for PoCA-based muon tomography techniques, it is an asset for muon radiography techniques. An added benefit of large amounts of high-Z materials to the muon radiography technique is the materials' ability to stop muons that hit them with up to 1 GeV of kinetic energy. This, along with the large angle deflections caused by the high-Z, high density materials, enables one to produce nice radiographs of waste and storage containers in much the same way as X-ray radiographic methods produce clear images of objects, such as airport luggage and the insides of a patient's lungs. Fig. 4, a radiographic image of the simulated DSC, is an example of the results obtained with "parallel beam" muon radiography. Parallel beam radiography involves using only muons whose initial trajectories are parallel to the vertical axis. The regions containing dark-colours demark the locations of the UO<sub>2</sub> fuel bundles. The light-coloured region, between the two rectangles of dark cells, clearly reveals the absence of two columns of fuel bundles.

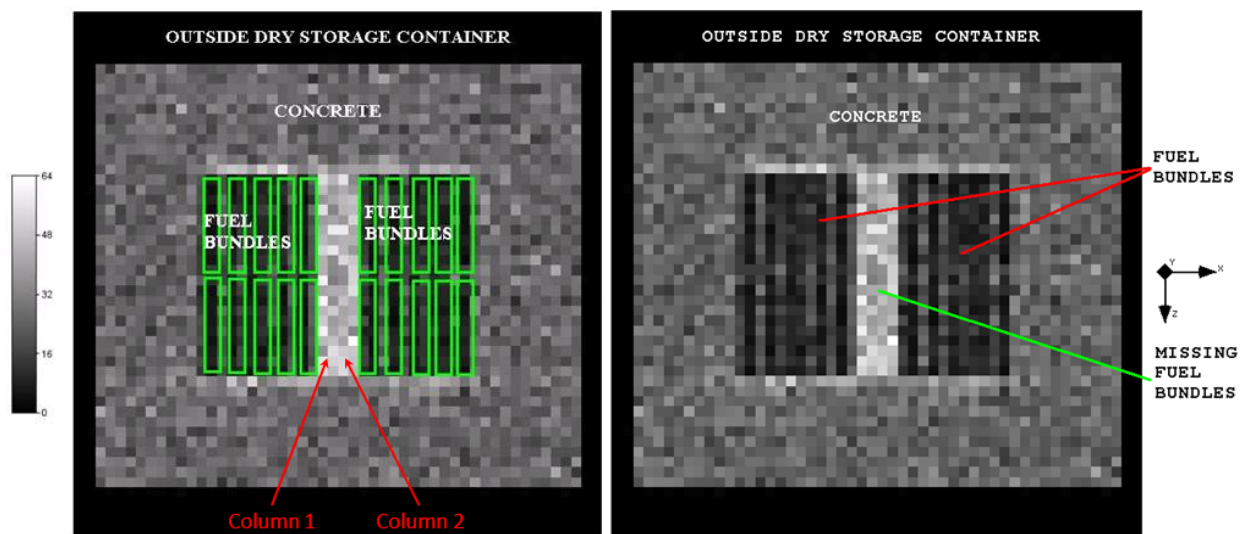


Fig. 4. A top view radiograph of the DSC. This image was generated via the parallel-beam muon radiography method. As was the case in the right-hand image of Fig. 2, two columns of fuel bundles were missing in this geometry. The simulations incorporated one day's worth of muons.

## CONCLUSIONS

A 55-gallon drum, containing PE (paraffin) and a  $\text{UO}_2$  fuel pin, and a DSC, made of concrete, and containing stacks of fuel bundles, were modeled in GEANT4. The multiple scattering of cosmic-ray muons in the drum and the DSC was simulated. GEANT4 wrote to an output file the hit positions and momentum vectors of the muons after they hit the argon planes placed above and below the object of interest. The hit positions and momentum vectors of the muons then entered into calculations of the muons' cumulative scattering angles and PoCA points. These values were then used to generate three-dimensional, tomographic images of the interiors of the drum and the DSC. The hit positions of muons that hit a bottom detector cell, directly below the cell they hit in the top detector, went into the creation of a two-dimensional, muon radiograph of the DSC.

The results of these image reconstruction efforts revealed the fact that PoCA-based muon tomography techniques are quite effective at imaging small amounts of high-Z material, enclosed within large volumes of low-Z material. Nevertheless, PoCA-based muon tomography yields poor imaging results for containers filled with large amounts of high-Z, high-density materials. Parallel-beam muon radiography, however, is quite effective at producing good images of the interiors of containers fill with large quantities of high-Z, high density substances. Based on the simulation studies, which this paper describes, both techniques provide effective methods to help characterise different types of materials in nuclear waste and storage containers.

One of the advantages of the Muon Tomography and Radiography techniques, which this paper explores, is that one need only measure the muons' tracks from one orientation of the object of interest. Given the promise of the two techniques, future simulations will be performed to determine the effects of finite detector position resolution on the tomographic and radiographic image qualities. There are also plans to simulate the more challenging situations posed by heterogeneous waste drum compositions, and to develop techniques that will enable one to differentiate between high-Z materials, like lead and tungsten, and fissionable actinides, like plutonium and uranium.

Finally, in order to implement the Muon Tomography and Radiography techniques, a sufficiently sturdy frame must be designed to hold the detectors and either a DSC or a waste container. In the case of DSC measurement, a device must be built to lift the DSC on the detector platform. DSC transport machines already exist, so building such a device should not be too difficult.

Ultimately, a potential use of muon radiography and tomography would be in their applications to characterisation of historical waste.

## REFERENCES

- [1] L. W. Alvarez et al., (1970). *Science* 167, 832.
- [2] Particle Data Group. "Review of Particle Physics," *Physics Letters*, B592 (2004), 1.
- [3] K. Borozdin, et. al., *Nature* 422 (2003) 277.
- [4] L.J. Schultz, et. al., Cosmic Ray Muon Radiography for Contraband Detection, Proceeding of AccApp'03, San Diego, CA, June 2003.
- [5] J. Donnard, Rapport de synthèse, Uppsala University, INF, (2004).
- [6] A. Flodin, Cosmic Muons for the detection of high-Z materials, Uppsala University, INF, UU-NF05 #4 (2005).
- [7] J. Gustafsson, Tomography of canisters for spent nuclear fuel using cosmic-ray muons, Uppsala University, INF, UU-NF05 #8 (2005).
- [8] C. Amsler et. al., Particle Data Group, *Review of Particle Physics, Physics Letters B* 667 (2008) 1.
- [9] M. Österlund *et al.*, International Workshop on Fast Neutron Detectors and Applications, Cape Town, South Africa, April 3-6, 2006.
- [10] W. C. H. Kupferschmidt, Managing Radioactive Waste at Atomic Energy of Canada Limited (AECL) – Recent developments, WM'05 Conference, Tucson AZ (2005).
- [11] W. C. H. Kupferschmidt and M. E. Stephens, AECL's Waste Management and Decommissioning Program, AECL.
- [12] IAEA Report, Strategy and Methodology for Radioactive Waste Characterization, IAEA-TECDOC-1537, March 2007.
- [13] <http://geant4.cern.ch/>
- [14] P.M. Jenneson, "Large vessel imaging using cosmic-ray muons", *Nuclear Instruments and Methods in Physics Research A* 525 (2004) 346–351.
- [15] M. Motoki et al., "Precise Measurements of Atmospheric Muon Fluxes with the BESS Spectrometer", *Astropart. Phys.*, 19 (2003), 113-126.